THE ASTROPHYSICAL JOURNAL, 305:417–432, 1986 June 1

MODELING OF CORONAL X-RAY EMISSION FROM ACTIVE COOL STARS. I. HYADES CLUSTER

ROBERT A. STERN[1]
Lockheed Palo Alto Research Laboratory
SPIRO K. ANTIOCHOS[1]
Naval Research Laboratory
AND
F. R. HARNDEN, JR.
Harvard-Smithsonian Center for Astrophysics
Received 1985 September 19; accepted 1985 November 26

ABSTRACT

X-ray pulse height spectra of the most active cool stars in the Hyades cluster obtained with the *Einstein* IPC cannot be satisfactorily fitted using isothermal thin plasma emission models. Addition of a second isothermal component provides acceptable fits. However, a more physically meaningful set of coronal parameters is provided by models which consist of an ensemble of loops with a single maximum temperature, but with the temperature distribution within the loop determined by loop physics. Such models have been successfully fitted to the IPC pulse height spectra. Constraints on loop parameters are discussed for the F–G dwarfs BD +14°693, BD +14°690, BD +15°640, and 71 Tau. Models with a large (>4) variation of loop cross section from base to top do not fit the data. A consistent physical description is an ensemble of small ($<10^{10}$ cm), high-pressure (>400 dynes cm^{-2}) loops of similar maximum temperature ($\sim$10–15 $\times$ 10^6 K for these stars) which dominate the coronal X-ray spectrum.

Subject headings: clusters: open — stars: coronae — stars: X-rays

I. INTRODUCTION

It is now more than a decade since the first X-ray emitting stellar corona was discovered (Catura, Acton, and Johnson 1975). Since then, rapid progress has been made in cataloging the incidence and range of stellar X-ray emission, most notably with the *Einstein Observatory* (*HEAO 2*; Giacconi *et al.* 1979). This wealth of data on coronal X-ray luminosities is in marked contrast to our limited information about stellar coronal structure (see, e.g., reviews by Stern 1983, 1984; Rosner, Golub, and Vaiana 1985). Coronal size can in principle be inferred in a few X-ray eclipsing binaries (e.g., Walter, Gibson, and Basri 1983). It may also be possible to use rotational modulation of single star X-ray emission in conjunction with similar Ca II variability (Baliunas *et al.* 1985) to obtain information on the sizes of stellar active regions. For the present, however, most stellar coronal models must rely on coronal temperature, emission measure, and pressure estimates derived from X-ray spectra.

Few stellar coronae have been observed spectroscopically. Several groups of researchers have tried to overcome this limitation by incorporating *International Ultraviolet Explorer* (*IUE*) observations of stellar chromospheres and transition regions between $\sim 3 \times 10^4$ K and 2×10^5 K with the X-ray data (Zolcinski *et al.* 1982; Landini *et al.* 1985; Giampapa *et al.* 1985). Stellar coronal models which make use of solarlike magnetic loops as "building blocks" (cf. Vaiana and Rosner 1978) can then be applied to the data under the assumptions that all loops have similar properties, and that the UV emission comes from lower temperature regions of the same loops that produce the X-ray emission. Leaving aside the question of simultaneity and other observational difficulties, constraints on loop base pressure and filling factor may be derived by assuming a given loop length and surface gravity. These results are somewhat encouraging, since many (but not all; see especially Giampapa *et al.* 1985) observations yield reasonable values for temperatures, filling factors, and loop pressures when modeled in this fashion.

Recently, however, new results from solar physics have appeared which suggest that a modified approach in constraining coronal model parameters is required. Feldman (1983), Rabin and Moore (1984), Athay (1984), and Antiochos and Noci (1986) all have argued for a decoupling of the lower transition region (TR) ($T < 10^5$ K) from the upper TR and corona. Their arguments are based on solar observations of spatial structure or derived emission measure distributions. Thus, although the heating processes for coronal loops and TR material should be physically related, the application of simple static loop models to connect the corona and TR may not be valid. While it is clear that the lower portions of coronal loops will contribute to stellar UV line emission, the integrated disk flux in each UV line may be dominated by low-lying, cooler "fine structure," mass flows, or cool loops with maximum temperatures below 10^5 K. Therefore, we are forced to rely on the X-ray spectrum for unambiguous coronal information.

The X-ray spectrum provides, at the very least, an estimate of an assumed isothermal coronal temperature. *Einstein* imaging proportional counter (IPC; Gorenstein, Harnden, and Fabricant 1981) data have relatively broad ($\Delta E/E \approx 100\%$ at 1.5 keV) energy resolution, but, given a spectrum with sufficient counting statistics (and after gain correction—see § III), the IPC has a wide enough energy response (0.2–4 keV) to estimate coronal temperatures in the 10^6 to several times 10^7 K range. In the vast majority of *Einstein* IPC coronal observations, the limiting counting statistics ensures that an isother-

[1] *Einstein* (*HEAO 2*) Guest Investigator.

mal model will fit the observed pulse height spectrum. However, for strong coronal sources, such as RS CVn systems, observations have been made with both the IPC (Majer *et al.* 1986) and the higher spectral resolution ($\Delta E/E \approx 10\%$–20%) solid state spectrometer (SSS), as well as the objective grating system (OGS; $\Delta E/E \approx 3\%$–20%). Typical results of such observations are that highly active stellar coronae ($L_x \approx 10^{31}$ ergs s^{-1}) are not well modeled by isothermal plasma emission, requiring at least two components with different temperatures, and in some cases, different emission measures (Swank *et al.* 1981; Mewe *et al.* 1982).

Can we ascribe any physical reality to such multiple-component models? A tempting answer is to assume that the coronal X-ray emission from the RS CVn systems comes from a mixture of "active" and "quiet" regions, as is the case for the Sun (Vaiana 1983). Once the temperatures of these two types of regions are specified, one can derive constraints on plasma parameters such as area coverage and "loop" length. There are in fact significant (factor of 2 or so) differences in the observed temperatures of solar quiet and active regions (Orral 1981), so at first glance the use of a two-component model is reasonable.

However, the loop structures observed in X-rays on the Sun are not isothermal. Therefore, attempting to constrain loop model parameters through the use of an isothermal approximation or even two delta functions in temperature, as in the two-temperature (2T) models, is unwise. Instead, we may first ask if there exists a class of single *maximum* temperature loop models whose predicted X-ray spectra are consistent with the available data. If so, what constraints can be derived from the application of such models to solarlike (and other classes of) stars? How do these compare with data from other wavelength regions and from solar observations?

Solar-type stars in the Hyades cluster are an obvious choice with which to begin such a study. The typical Hyades G dwarf star has an X-ray luminosity $L_x \sim 50$ times solar, and the brightest Hyades G star coronae are more than ~ 100 times the solar L_x. At the Hyades distance, a star with $L_x \approx 10^{30}$ ergs s^{-1} produces ~ 2000 IPC counts in a 10,000 s exposure. In the original Hyades X-ray survey with the *Einstein* IPC (Stern *et al.* 1981), we identified a number of candidates using ~ 2000 s exposures for such longer follow-up observations. Some of the results from these follow-up observations have been reported elsewhere by Stern and Zolcinski (1983), Zolcinski and Stern (1985), and, in the case of a stellar flare, by Stern, Underwood, and Antiochos (1983). The recent reprocessing (Harnden *et al.* 1984) of *Einstein* IPC spectral data has enabled us to confidently fit IPC pulse height information. In this paper we concentrate on the IPC spectral observations of a selected group of Hyades stars and the application of isothermal, two-temperature, and more realistic hydrostatic loop models to the data, in an effort to identify the fundamental properties of solar-type active stellar coronae.

II. OBSERVATIONS

All observations were carried out using the IPC. Table 1 lists the individual fields, pointing directions, and stellar characteristics. The selection of target stars was made based on the results of the initial Hyades cluster survey of Stern *et al.* (1981). Given the requirement of $\sim 10{,}000$ s exposure times to obtain adequate counting statistics, we were limited to the brightest X-ray objects in the cluster. Placement of the sources at the center of the field was required because of the detector gain uncertainty for point sources outside a central $4' \times 4'$ region (Harnden *et al.* 1984).

All spectral data were derived using the *Einstein Observatory* Revision 1 software (Harnden *et al.* 1984), which explicitly corrects for the high spatial frequency IPC gain variations of the targeted objects. Although the energy resolution of the IPC is only $\sim 100\%$ FWHM at 1.5 keV (Gorenstein, Harnden, and Fabricant 1981), the combination of adequate count rate statistics and accurately determined counter gain allows the determination of constraints on various model parameters using χ^2 goodness-of-fit and parameter estimation procedures (e.g., Lampton, Margon, and Bowyer 1976; Cash 1976).

As part of the Rev. 1 production processing software, targeted objects at the center of the IPC fields are automatically fitted to simple X-ray emission models assuming power-law and exponential spectra, with various assumed interstellar column densities. Although in most cases adequate fits were found to the IPC observations, we have not considered further analysis of the data using such simplistic models to be useful, for the following reasons: (1) As discussed in Stern *et al.* (1981), the incidence of X-ray sources as a function of spectral type and their derived X-ray luminosities make it highly unlikely that they are anything but stellar coronae; hence the power-law models are physically unrealistic. (2) The use of a simple exponential, while it approximates a pure H bremsstrahlung spectrum, is also unrealistic, since the atmospheres of the stars in question are known to have abundances very similar to

TABLE 1

OPTICAL CHARACTERISTICS

Field Number	VB[a] Number	Other Designation	HD	Sp.	V	$B-V$	R.A.	Decl.	Notes
I9001.....	64	BD +16°601	28099	G6 V	8.1	0.66	$4^h23^m48^s0$	16°38′08″	
I9002.....	40	BD +14°690	27691AB	G0 V	7.0	0.56	4 19 54.0	14 56 25	b
I9003.....	50	BD +14°693	27836	G1 V	7.6	0.60	4 21 22.0	14 38 38	
I9004.....	141	71 Tau	28052	F0 V	4.5	0.25	4 23 30.0	15 30 23	
				+ G4 V?	+8.1?				c
I9005.....	71	θ^1 Tau	28307	K0 III	3.9	0.96	4 25 43.0	15 51 10	
				+ F8 V?	+7.4?				d
I9006.....	85	BD +15°640	28568	F5 V	6.5	0.42	4 27 55.0	16 02 30	e

[a] Van Bueren 1952.
[b] Spectroscopic binary, $P = 4$ days.
[c] Evidence of G4 V wide companion from lunar occultation; (Peterson *et al.* 1981).
[d] Evidence of F8 V wide companion from lunar occultation; (Peterson *et al.* 1981).
[e] Evidence of variability during exposure (Zolcinski and Stern 1985).

TABLE 2

SUMMARY OF OBSERVATIONS AND BEST-FIT ISOTHERMAL MODELS

Source	Date of Observation	Exposure Time (s)	Total Counts	Temperature (keV)	χ^2	Degrees of Freedom	Confidence Level
BD +16°601	1980 Sep 18	12826.	249	0.35	1.9	5	0.85
BD +14°690	1981 Jan 30	8369.	502	0.32	14.4	8	0.08
BD +14°693	1981 Jan 30	9380.	11119	0.45	37.	9	<0.001
71 Tau	1980 Sep 19	10811.	2514	0.90	52.	8	<0.001
θ^1 Tau	1981 Jan 30	9461.	1270	0.40	27.	8	<0.001
BD +15°640	1981 Jan 31	11648.	685	2.2	19.	7	<0.01

solar abundances, if only slightly more metal-rich (see § IV); thus temperature limits derived in this approximation are useful only as order-of-magnitude indicators. (3) In many cases the required best-fit hydrogen column densities are in conflict with observational upper limits. We therefore base the analysis that follows on models using cosmic or near-cosmic abundance plasma emissivities.

The question of variability during an exposure also arises. Only one of the stars, BD +15°640, exhibited significant (~25%) X-ray flux variability during the observations (another of the target stars, BD +14°690, exhibited flaring behavior in a later observation; Zolcinski and Stern 1985). Even in the case of BD +15°640, the variation of X-ray emission was not characteristic of a single, flarelike event, in contrast to that seen in HD 27130 (Stern, Underwood, and Antiochos 1983). This does not rule out the possibility of continual "miniflares" from regions on the stellar disk producing an apparent steady state emission light curve (see, e.g., Stern and Skumanich 1983). However, in the absence of any conclusive evidence for such a continually flaring corona, we will proceed under the assumption that the X-ray light curves are consistent with quasi-static coronal heating.

III. ISOTHERMAL PLASMA ANALYSIS

We began our analysis by fitting models of an isothermal plasma spectrum (Raymond and Smith 1977; Raymond 1979). The model is parameterized by a temperature (kT) and an emission measure ($\int N_e^2\, dV$). We have assumed that interstellar absorption is negligible, since equivalent hydrogen column densities of less than 10^{19} cm^{-2} or so estimated for the Hyades ($d = 45$ pc) are unlikely to affect the X-ray data (see Stern *et al.* 1981). The fitting results are summarized in Table 2 for the central stars in the observing fields, including net exposure times for the fitted spectra and observing dates. It is quite apparent that, except for the observation of BD +16°601 with poor count rate statistics, the data are not well fitted by isothermal plasma models. We note here that similar results have been found for the RS CVn systems both by Swank *et al.* (1981) using higher spectral resolution SSS data, and by Majer *et al.* (1986) using IPC data.

Because the metal abundance in the Hyades is higher than solar ([Fe/H] ≈ 0.2 dex; Branch, Lambert, and Tomkin 1980), we have also fitted the IPC spectra to models with Fe abundance of up to 2 times solar. Since much of the X-ray flux near 1 keV comes from Fe ions at $T \approx 10^6$–10^7 K, increasing the Fe abundance relative to H significantly affects the predicted spectra. However, the effect is clearly to enhance the emissivity near 1 keV relative to higher and lower energies: this is exactly the opposite effect needed to satisfactorily fit the IPC spectra. The results of these isothermal models with enhanced Fe abundance are, in all cases, poorer than the original solar abundance fits.

IV. TWO-TEMPERATURE MODELS

Following the example set by the RS CVn analysis, we then proceeded to fit our spectral data with 2T plasma models. Such models are parameterized by the two temperatures and two emission measures (or equivalently, an emission measure ratio and overall X-ray flux). The results of such two-temperature fits are given in Table 3, with 90% confidence χ^2 contour intervals for the two temperature components shown in Figure 1. A comparison of the best-fit single-temperature and 2T models is shown for the star BD +14°693 in Figure 2. Several important points should be noted:

1. The models in general provide very good formal fits to the data.
2. Although the individual temperatures are poorly constrained, the fits generally require one temperature $\lesssim$ a few million degrees, and the other ~10–20 × 10^6 K.
3. For most of the stars (except BD +15°640, which was slowly variable during the observing period), the best fits require more emission measure at the higher temperature. However, the emission measure ratio is a strong function of the pair of temperatures selected: the poor constraints on temperature yield equally poor constraints on emission measure ratio.

TABLE 3

BEST-FIT 2T MODELS

Source[a]	kT_1 (keV)	kT_2 (keV)	χ^2/Degrees of Freedom	Level of Confidence	EM_1/EM_2	log (EM_2) (cm^{-5})
BD +14°693	0.31	4.5	4.0/7	0.80	0.38	52.4
BD +15°640	0.03	1.1	8.1/5	0.20[b]	4.8	51.8
BD +14°690	0.26	2.0	5.9/7	0.40	0.6	51.9
71 Tau	0.15	1.3	6.2/8	0.50	0.14	52.4
θ^1 Tau	0.07	1.0	7.4/7	0.62	0.3	52.2

[a] BD +16°601 not included; isothermal model provided good fit.
[b] Variable during exposure.

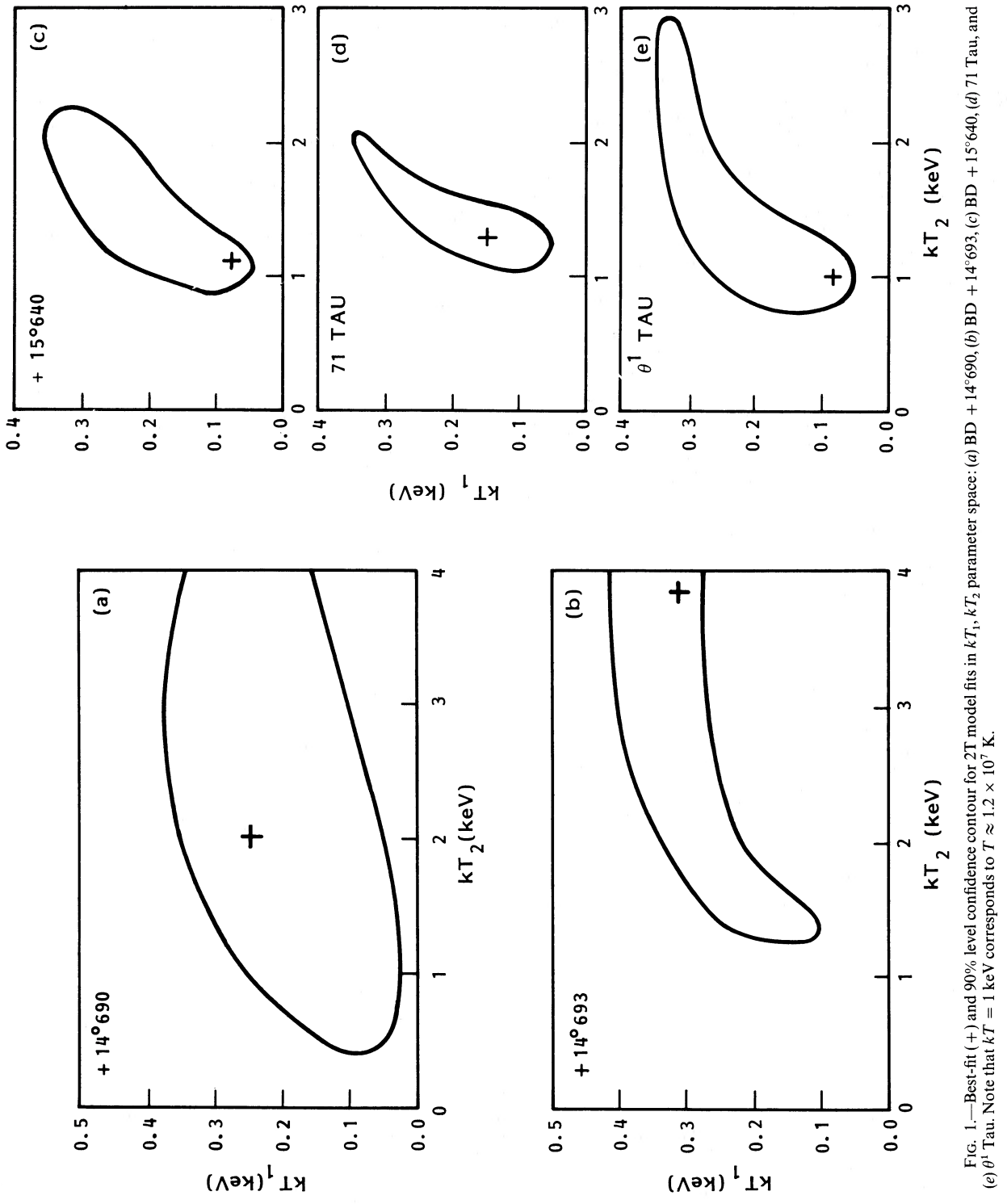

FIG. 1.—Best-fit (+) and 90% level confidence contour for 2T model fits in kT_1, kT_2 parameter space: (*a*) BD +14°690, (*b*) BD +14°693, (*c*) BD +15°640, (*d*) 71 Tau, and (*e*) θ^1 Tau. Note that $kT = 1$ keV corresponds to $T \approx 1.2 \times 10^7$ K.

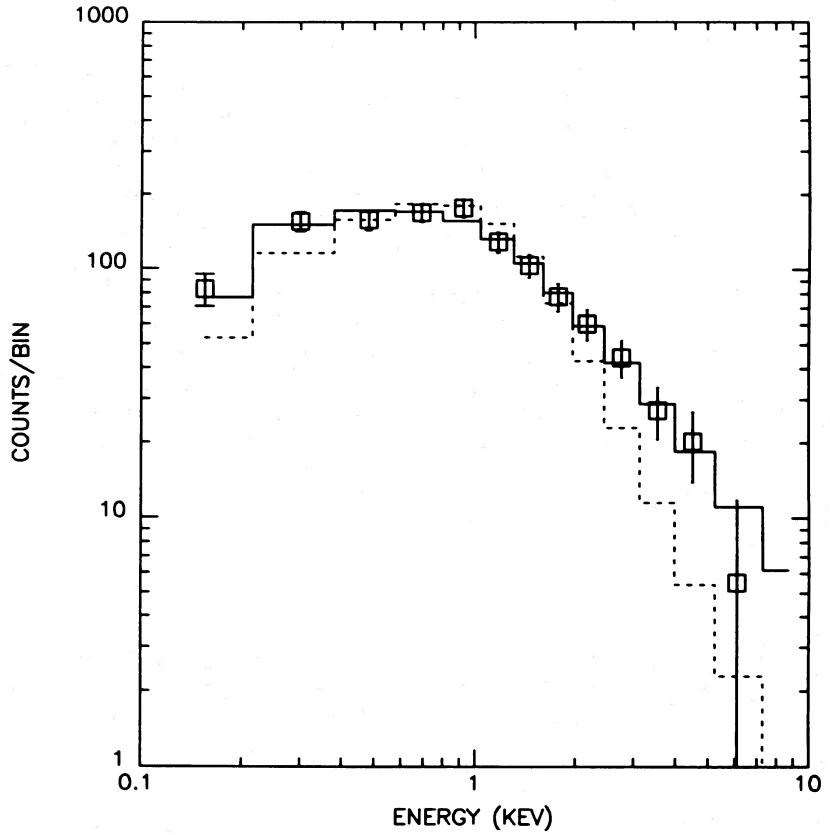

FIG. 2.—Predicted IPC pulse height spectra for best-fit single-T model (*dashed line*) and best-fit 2T model (*solid line*) for BD +14°693. Observed IPC spectrum is shown by points with error bars of $\pm 1\ \sigma$.

We note also that the limits we have derived on the temperature of each component in this model approximation are significantly affected by instrument characteristics. Specifically, the IPC window transmission function contains the C_K edge at $E \approx 0.28$ keV. Hence, the observed counts appearing in the $\sim$0.3–0.5 keV energy bins are due primarily to photons at higher or lower energies because of the wide (>100%) energy response of the counter coupled with the high opacity of the window. In their analysis of IPC RS CVn spectra, Majer *et al.* (1986) noted that while both the SSS and IPC spectra of a given RS CVn system could be separately fitted by a 2T model, the temperatures in each case differed significantly, which suggested a *continuous* temperature distribution. Although we have no SSS spectra of Hyades stars, we believe it likely that a similar situation exists in our IPC data. Therefore, our principal conclusion from the 2T model fits is that all the stars examined (the four F–G dwarfs and the giant θ^1 Tau) must have a significant emission measure at $kT \gtrsim 0.3$–0.5 keV. In all but the case of BD +15°640, this is similar to or greater than that at lower temperatures (see Table 3). Thus, although the 2T models should not be taken too literally, they are an important indication of emitting material approaching flarelike temperatures in the most active Hyades stars.

V. LOOP MODEL ANALYSIS WITH PREDICTED EMISSION MEASURE DISTRIBUTION

a) Modeling Approach

Although the model fits described in the previous section provide good formal fits to the data, the derived parameters are not easy to interpret physically. If we assume that the two components are magnetic loop ensembles of differing temperatures, we are confronted by a fundamental inconsistency of the analysis: in hydrostatic or dynamic loop models (e.g., Vesecky, Antiochos, and Underwood 1979) the temperature distribution in a single loop is not isothermal; hence the models used to fit the data are physically unrealistic. Thus derived surface coverages or pressures for a two-component corona are likely to be unreliable.

The limited spectral resolution of the IPC is insufficient to single out contributions from individual X-ray lines and thereby better constrain the emission measure distribution. However, under the assumption of a hydrostatic, magnetically confined plasma, the balance of heating, thermal conduction, and radiation will fix the temperature distribution given a loop length, heating rate, and geometrical properties (see below). By using basic physics to constrain the relationships among loop parameters, and by examining model X-ray spectra derived under these constraints, we may gain greater insight into coronal structure.

We proceeded to generate a grid of loop models, fold the resulting emission measure distribution through the Raymond (1979) plasma emissivity models, and integrate the derived emission along the loop to produce an emergent spectrum. The purpose of such an analysis is first to see if the IPC data can be modeled by an ensemble of loops with the same maximum temperature T_{max} before seeking an interpretation invoking a two-component corona.

Schmitt *et al.* (1985) took a similar approach with IPC data

on Procyon (F5 IV + WD), deriving a log $T_{max} \approx 6.2$. However, they only considered the case of constant cross section loops. The variation of the loop cross section, as we shall see below, is the other major factor besides T_{max} that strongly influences the loop emission measure distribution. Also, Schmitt *et al.* found adequate fits to their IPC data with isothermal models and thus were not forced into examining more complicated temperature distributions, as we were. However, we strongly believe that adopting an approach using coronal loop models, as discussed here and in Schmitt *et al.* (1985), provides considerably more insight into coronal physics than the isothermal or 2T models discussed above. We note also that the principal differences between our analysis and those of Zolcinski *et al.* (1982); Landini *et al.* (1985); Landini, Monsignori Fossi, and Pallavacini (1985); and Giampapa *et al.* (1985), is that the IPC pulse-height data and not just total X-ray flux provide most of the constraints in our case, with additional constraints coming from the C IV observations used as upper limits only; we also have not used UV lines formed at lower temperatures for the reasons mentioned in § I.

b) *Loop Model Formulation and Derived Plasma Emission Spectrum*

We used the numerical code developed by Vesecky, Antiochos, and Underwood (1979) to calculate hydrostatic solar loop models. In the limit of low gravity and constant loop cross section, this numerical code yields results equivalent to the analytical formulations of previous researchers (e.g., Landini and Monsignori Fossi 1975; Rosner, Tucker, and Vaiana 1978); it has the advantage of being able to incorporate both the effects of stellar gravity and variable loop cross section. In addition, the derived emission measure distribution can easily be folded in numerically with the plasma emissivity at each temperature interval to derive a emergent model spectrum.

Each loop model is obtained by solving the standard one-dimensional equilibrium equations (see, e.g., Vesecky, Antiochos, and Underwood 1979). These are the equation of hydrostatic equilibrium:

$$\frac{dp}{ds} = \rho g_{\|}(s) \tag{1}$$

and the equation of energy balance:

$$\frac{1}{A(s)} \frac{d}{ds} [A(s)F_c] = -N_e^2 \Lambda(T) + \epsilon \, . \tag{2}$$

In equations (1) and (2), s is the distance along the loop, i.e., along the magnetic field line; $g_{\|}$ is the component of gravity parallel to the field; F_c is the conductive flux; $A(s)$ is the loop cross-sectional area; $\Lambda(T)$ is the radiative loss coefficient; ϵ is the coronal heating rate, assumed constant per unit volume throughout the loop; p is the pressure at s; ρ is the density; and N_e is the electron density at s. We use the Spitzer conductivity so that the heat flux is given by

$$F_c = -10^{-6} T^{5/2} \frac{dT}{ds} \, . \tag{3}$$

The functions $g_{\|}(s)$ and $A(s)$ are determined by the magnetic field geometry. We assume the field to be that due to a line dipole at some depth below the chromosphere. Given a known stellar radius, the complete loop geometry (including line dipole depth) is determined by the loop length L and the ratio of the area at the apex to that at the base, which we designate Γ. This latter quantity measures the total coronal expansion of the flux tube. For fixed values of L and Γ, the plasma emission measure distribution is relatively unaffected by variations in the detailed form of $g_{\|}$ or $A(s)$; hence, the results for the line dipole case should have quite general validity. Exact expressions for $g_{\|}$ and A are given in Vesecky, Antiochos, and Underwood (1979). The loop model geometry is shown in Figure 3.

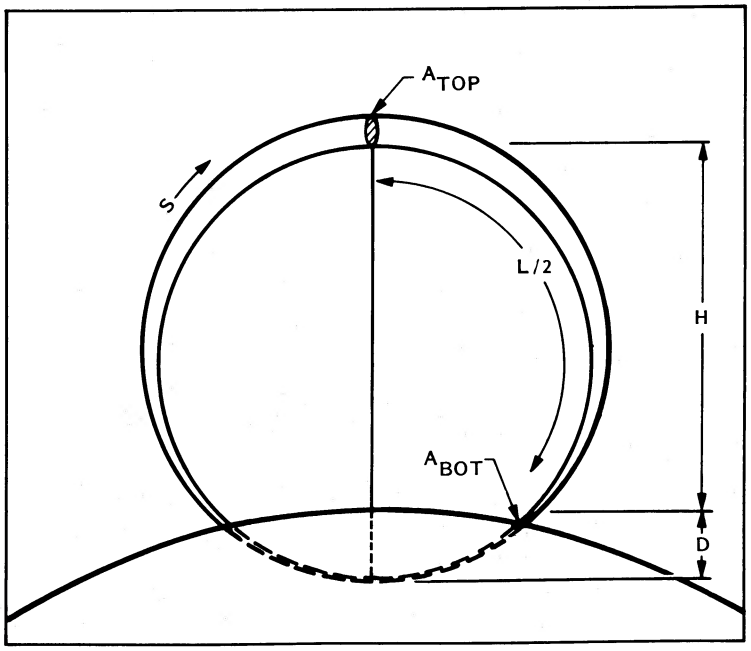

FIG. 3.—Loop model geometry: dashed lines indicate region below stellar chromosphere. $\Gamma = A(\text{top})/A(\text{bottom})$

Along with equations (2) and (3), boundary conditions must be specified at the loop base. We assume that the base temperature is fixed to be 3×10^4 K and that the heat flux vanishes there. The numerical code uses these conditions as initial values to integrate equations (2) and (3) and obtain the run of temperature and density along the loop, $T(s)$ and $n(s)$. The differential emission measure, expressed as a function of temperature, is obtained from

$$\xi[T(s)] = A(s)N_e^2(s)\left|\frac{d \ln T}{ds}\right|^{-1}. \quad (4)$$

The X-ray spectrum can then be predicted by convolving ξ with the plasma emissivity calculations of Raymond and Smith (1977), revised by Raymond (1979):

$$\frac{dN}{dEdt} = \int \xi(T)\frac{P(T, E)/N_e^2}{E} d(\ln T), \quad (5)$$

where E is the photon energy, P/N_e^2 is the emissivity function, and the range of the integral is over all temperatures in the loop. Note that since the plasma is assumed to be optically thin (an assumption likely to be correct for all but a few of the strongest X-ray lines), the direction of observation does not affect the emergent spectrum.

An important consideration is the number of free parameters in the models. We assume at the outset that the emission from any particular star originates from an ensemble of identical loops. This is clearly both the simplest modeling approach, and, at the same time, the one that provides the most stringent constraint that can be placed on the models. In reality, a corona must consist of a distribution of loops with different geometries, temperatures, and densities; however, the X-ray data are insufficient to support an analysis in terms of such a distribution. In addition, it appears from solar observations that the coronal emission may indeed be dominated by a few of the highest temperature loops (see § VI), so that our assumption is not without foundation.

With this assumption, then, the number of parameters needed to completely specify a stellar corona, and consequently a predicted X-ray spectrum, is no more than four: the heating rate ϵ, the length of each loop L, the expansion factor Γ, and the total emitting area. It is convenient to parameterize this latter quantity by the filling factor f, the fraction of the stellar surface that is covered by loop footpoints. In terms of f, the X-ray spectrum observed at earth is

$$I(\mathrm{E}) = \left(\frac{R_*}{d_*}\right)^2 f\Gamma \frac{dN}{dEdt} \text{ photons cm}^{-2}\text{ s}^{-1}\text{ keV}^{-1}, \quad (6)$$

where R_* is the stellar radius, d_* is the stellar distance, and the other quantities have been defined previously. The area $A(s)$, which appears in the differential emission measure (4), is normalized to unity at the loop top, i.e., $A(\text{top}) = 1$ cm^2. It is also more convenient to replace ϵ as a parameter by the maximum temperature in the loop $T_{\max}$. These two quantities are perfectly interchangeable: for fixed values of L and Γ, there is a one-to-one relation between ϵ and $T_{\max}$. Since the temperature is the quantity that is more closely related to the observations, we may as well use it instead of ϵ. As a final point, we note that the total number of parameters in the single $T_{\max}$ loop model (four: ϵ or $T_{\max}$, L, Γ, and f) is the same as the total number of parameters for the 2T model (T_1, T_2, EM_1, and EM_2). Thus we have not introduced any more free parameters in the loop model formulation. In fact, as we see below, under most circumstances the predicted X-ray spectrum depends primarily on the values of $T_{\max}$, Γ, and f; thus the loop model formulation actually has fewer free parameters than the 2T models.

TABLE 4

LOOP MODEL PARAMETER RANGES

$T_{\max}$ (10^6 K)	L (10^{10} cm)	Γ
7.....	0.1, 1., 10.	2, 5, 10
10.....	0.1, 1., 5., 10., 20.	2, 5, 10
15.....	0.1, 0.5, 1., 5., 10., 20.	1.001, 2, 5, 10, 20, 50, 100
25.....	0.1, 1., 10.	2, 5, 10

c) *Application of Loop Models to IPC Spectral Fits*

We have generated a grid of 74 loop models using the numerical code described in Vesecky, Antiochos, and Underwood (1979) with parameter ranges listed in Table 4. Note that the maximum temperature of the loop models was kept as constant as possible for a given range of L and Γ by varying the heat input rate ϵ. As indicated above, the maximum temperature could be estimated at first from the results of the 2T model fits and then varied, keeping the other parameters the same, to see its effect on the goodness of fit. An example of the run of pressure, temperature, and emission measure of the loop models so constructed for differing values of Γ is shown in Figure 4.

The loop models were applied to the four dwarf stars 71 Tau, BD +14°693, +15°640, and +14°690. The results of the best-fit loop models are shown in Table 5. An example of the best-fit IPC spectrum for a loop model is shown in Figure 5 for BD +14°693. Note that the best-fit χ^2/degree of freedom for the loop models are similar to those obtained for the 2T

TABLE 5

BEST-FIT LOOP MODEL PARAMETERS

Source	χ^2(min)	Degrees of Freedom	T (10^6 K)	L (10^{10} cm)	Γ	P (dynes cm^{-2})	f	Note
BD +14°693	7.9	9	15	10.	2	45	2.6	a
	8.2	9	15	1.	1	290	0.43	
BD +14°690	9.5	9	10	10.	2	12	7.0	a
	10.8	9	7	0.1	2	210	0.37	
BD +15°640	11.8	9	15	0.1	1	2900	0.02	
71 Tau	7.7	9	15	5.	2	80	2.8	a
	8.6	9	15	1.	2	370	0.54	

[a] Best fit has surface coverage >1; next best fit indicated on 2nd line.

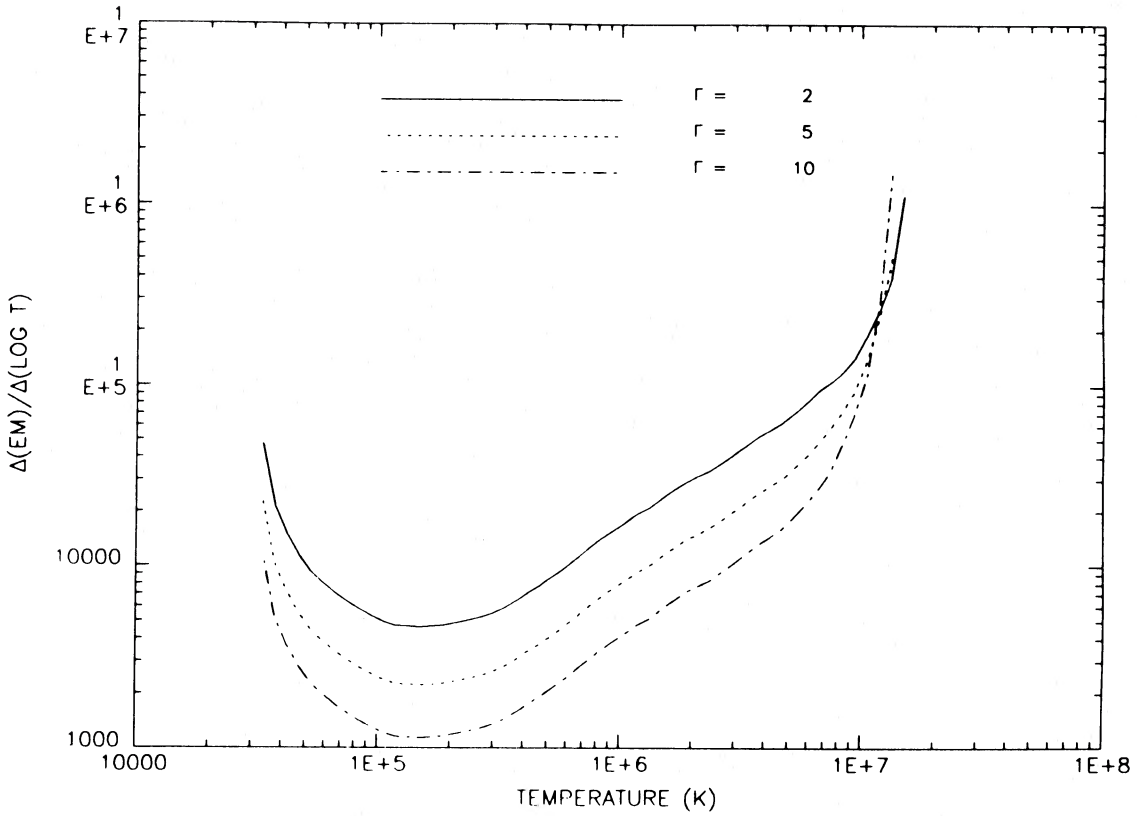

FIG. 4.—Differential emission measure distribution as a function of temperature along the loop computed using loop model parameters $T_{max} = 15 \times 10^6$ K, $L = 10^{10}$ cm, for $\Gamma = 2, 5, 10$.

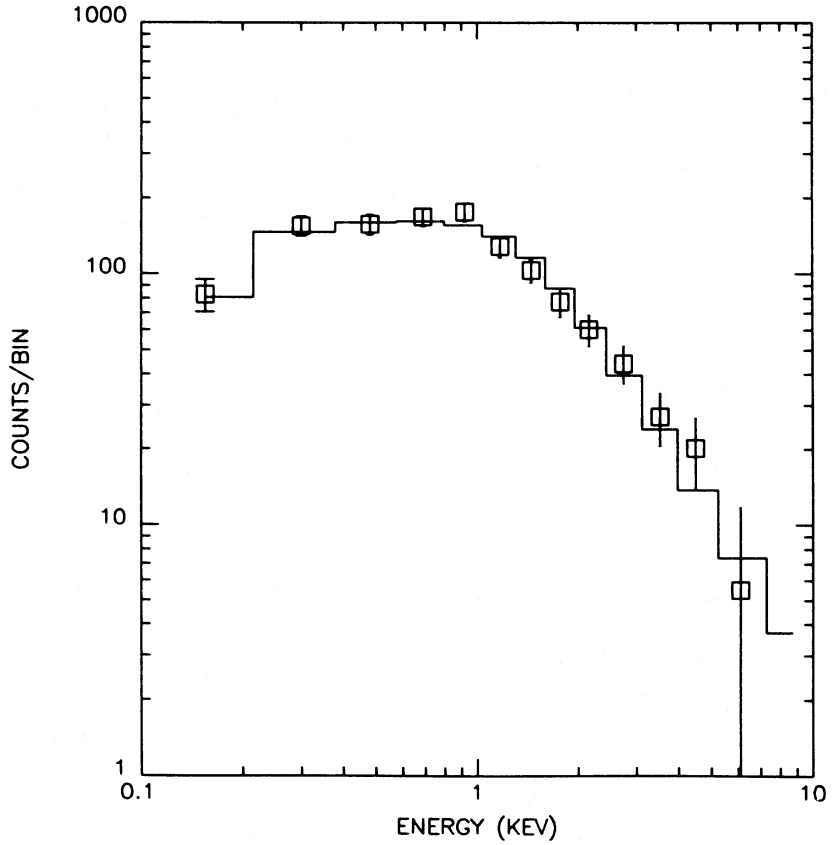

FIG. 5.—Best-fit predicted loop model IPC pulse height spectrum for BD +14°693 compared to observations

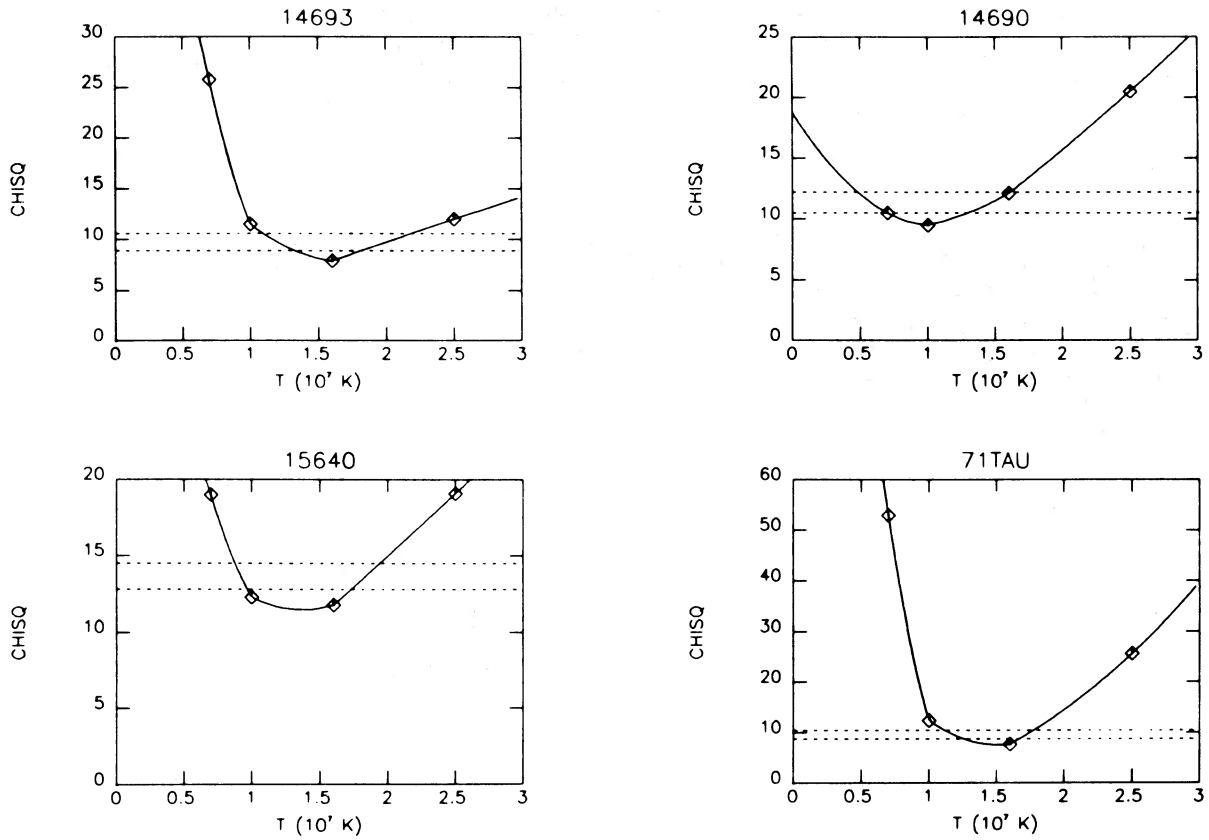

FIG. 6.—χ^2 vs. maximum loop temperature for four dwarf stars. The dashed lines indicate 68% and 90% χ^2 confidence intervals for T_{max}.

model formulation and that both of these are considerably better that the isothermal model fits.

d) Constraints on Loop Model Parameters

The most apparent constraint on loop model parameters for the fitted IPC spectra is on T_{max}, the maximum coronal temperature. In Figure 6 we have plotted the χ^2 value of the best-fit loop model for a given T_{max} (i.e., ϵ), allowing the other parameters (Γ, L, and f) to minimize χ^2, for the four dwarf stars. The range of allowable maximum loop temperatures is fairly narrow, $\sim$10–25 $\times$ 10^6 K. We note that the best-fit temperature for the F0 dwarf 71 Tau is indistinguishable from that of the G dwarfs, as are constraints on most of the other parameters. Since 71 Tau has a faint G4 V companion identified in a lunar occultation (see Table 1), it is very likely that the G star is producing some of the X-ray flux.

At the best-fit temperatures for each of the dwarf stars, we plot in Fig. 7 the χ^2 contours in $\Gamma - L$ parameter space for confidence levels of 68%, 90%, and 99% (two parameters jointly estimated; Cash 1976). Also plotted in Figure 7 are contours of constant f, derived from equation (6) above. Since $f > 1$ is physically unrealizable, we may use this constraint along with the limits set by χ^2 to derive a maximum Γ and loop length L for each star. These are given in Table 6.

Plotted in Fig. 8 are contours of constant loop base pressure for loops with $T_{max} = 10$ and 15 $\times$ 10^6 K respectively. The base pressure is completely determined once T_{max}, Γ, and L are specified in the loop model. Using the constraints on L and Γ above, we may then derive a minimum base pressure for each star, assuming loops of this length completely cover the stellar disk. These results are also indicated in Table 6. The pressure at the loop top is virtually identical to the base pressure except for loops long compared to the coronal scale height (5 $\times$ 10^{10} cm for $T \approx 10^7$ K).

TABLE 6

LIMITS ON LOOP MODEL PARAMETERS SET BY COVERAGE FRACTION

		f(X-ray) < 1			f(X-ray) < f(C IV) < 1	
STAR	Sp.	Γ_{max}	L_{max} (10^{10} cm)	P_{min} (dynes cm^{-2})	L_{max} (10^{10} cm)	P_{min} (dynes cm^{-2})
BD +14°693	G1 V	3	5	100	2	200
BD +15°640	F5 V	4	10	45	3	100
BD +14°690	G0 V	4	0.3	400	...	...
71 Tau	F0 V	2.5	2	250	...	...

NOTE.—Derived using 90% confidence contours for Γ vs. L.

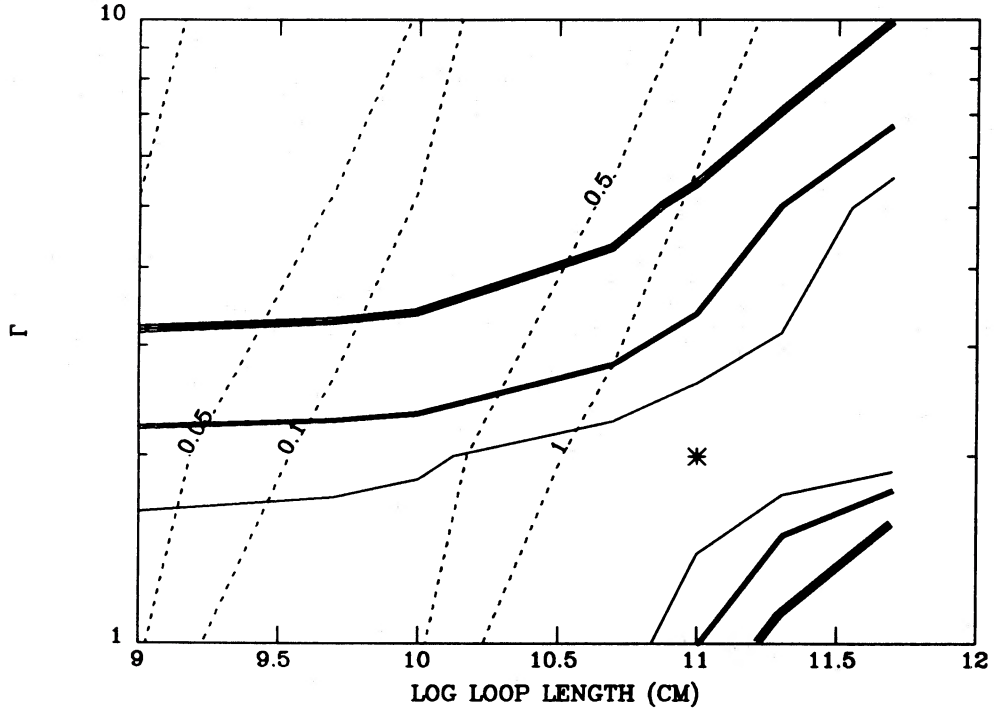

FIG. 7*a*

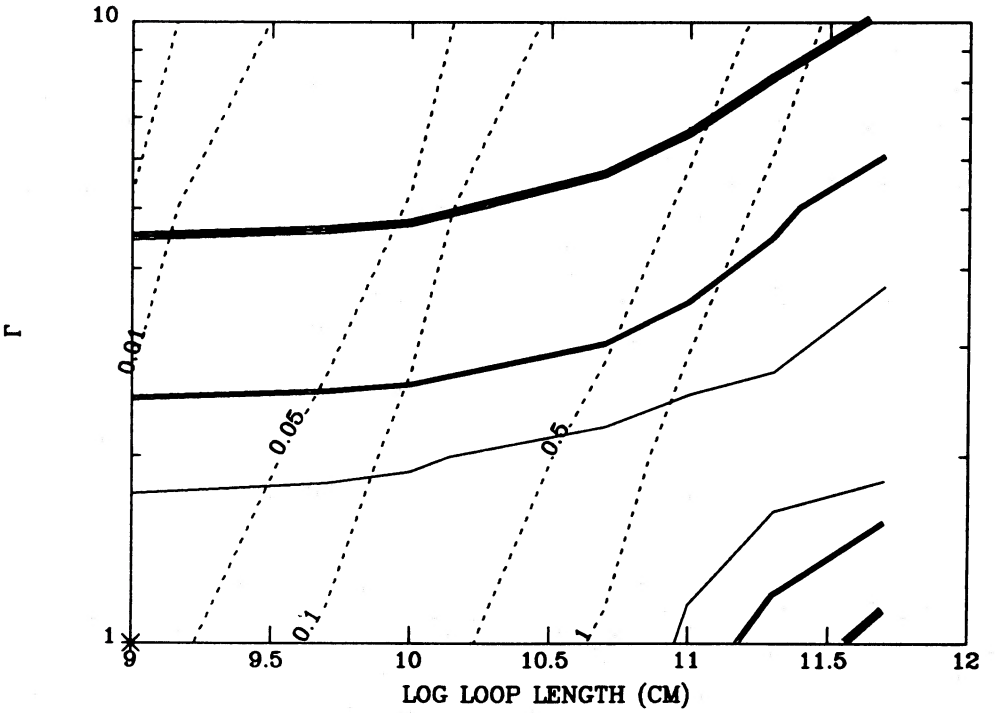

FIG. 7*b*

FIG. 7.—χ^2 contours for model fits to (*a*) BD +14°693, (*b*) BD +15°640, (*c*) BD +14°690, and (*d*) 71 Tau. The star indicates minimum χ^2, and solid lines of increasing thickness are contours for 68%, 90%, and 99% confidence levels in the (Γ, L)-plane. Dashed lines are labeled contours of constant surface coverage factor f in the (Γ, L)-plane. In (*c*), model fits were only available for $\Gamma > 2$.

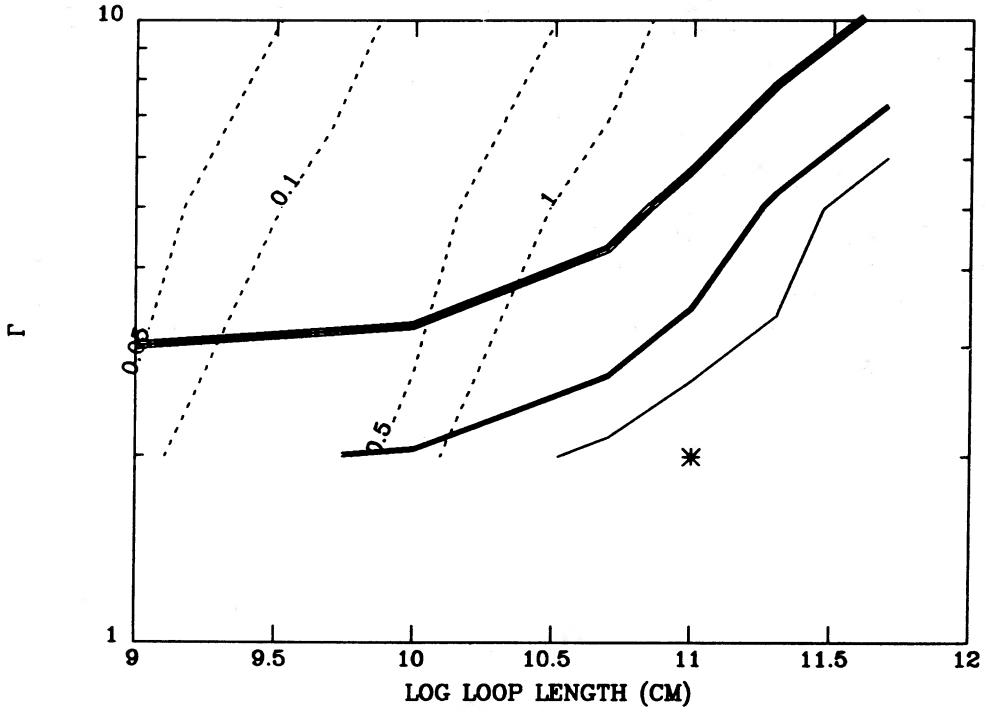

FIG. 7*c*

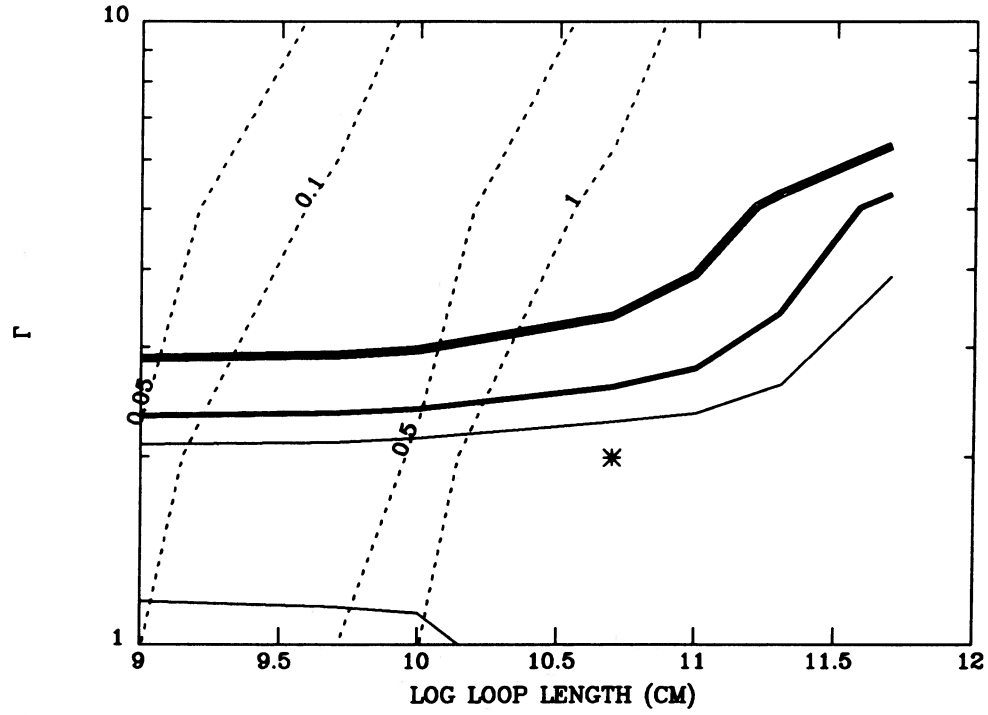

FIG. 7*d*

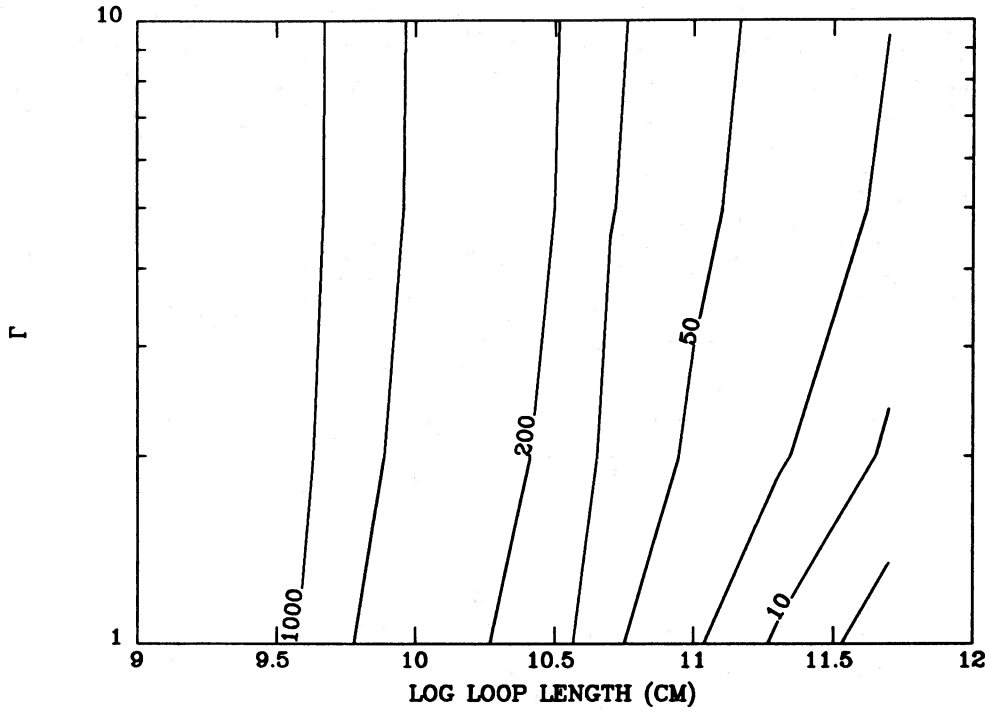

FIG. 8*a*

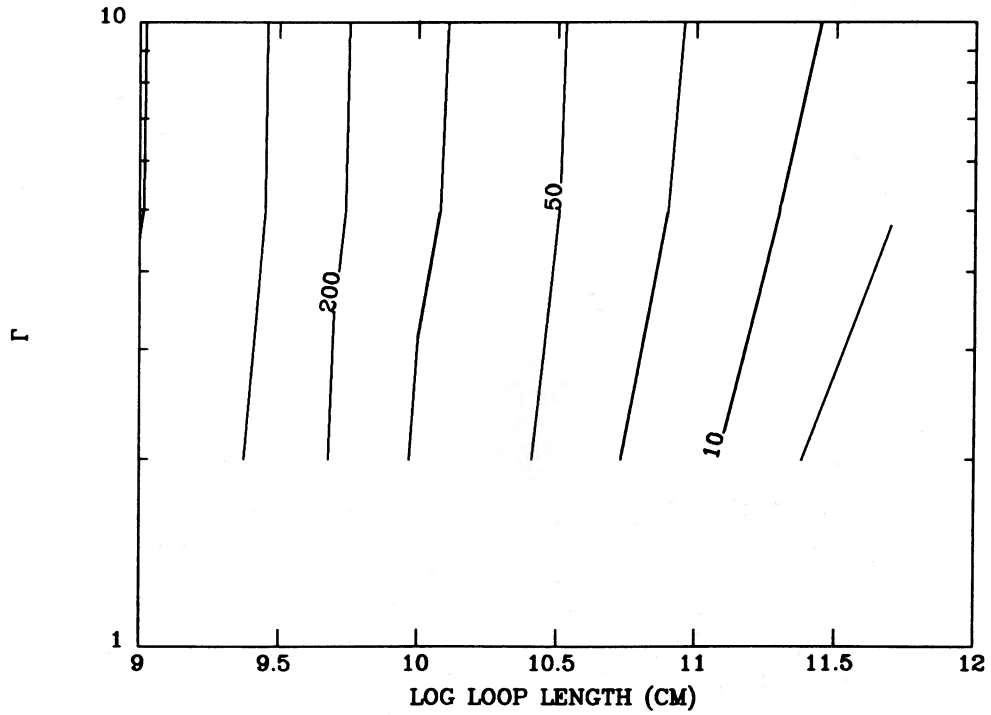

FIG. 8*b*

FIG. 8.—Contours of constant loop base pressure (dynes cm^{-2}) in the (Γ, L)-plane for models with T_{max} = (*a*) 15 × 10^6 K and (*b*) 10 × 10^6 K

VI. DISCUSSION

The results of the previous section demonstrate that a class of single maximum-temperature loop models exists which fit the IPC pulse height spectra of active Hyades stars. Keeping in mind the lack of spatial and spectral resolution inherent in these data, we may proceed to compare these models to solar coronal loop structures. Our purpose will be to draw some general conclusions about coronal structure in the Hyades stars and to see which results are somewhat less model-specific than others. We reiterate that, although the 2T model of loop emission measure will represent the data equally well, a physically self-consistent "2T" loop model should have ensembles of single T_{max} loops: the results of the previous section show that such a second ensemble of loops is not required.

The first point to note is that T_{max} for these stars is similar to that seen in solar flares. We note also that T_{max} in the loop models (or the higher T in the "2T" models) is comparable to that seen in the RS CVn systems by Swank *et al.* (1981) and Majer *et al.* (1986). The large value for T_{max} suggests that the coronal heating rate is larger in the Hyades dwarfs than in the Sun. Using the scaling laws for coronal loops (e.g., Rosner, Tucker, and Vaiana 1978; Vesecky, Antiochos, and Underwood 1979), we can relate T_{max}, ϵ, and L:

$$T_{max} \approx \epsilon^{2/7} L^{4/7} . \quad (7)$$

Hence, to increase T_{max} either ϵ or the loop length L must increase. Our results of the previous section show that L is unlikely to be larger than for solar active regions, so that ϵ must increase. Note also that this increase must be quite large, since T_{max} is approximately an order of magnitude larger in the Hyades. We therefore deduce that the heating rate is at least three orders of magnitude larger in these stars than in the Sun. Furthermore, since in most theories of coronal heating $\epsilon \approx B^2$ (Tucker 1973; Rosner *et al.* 1978; Golub *et al.* 1980; Sturrock and Uchida 1981; Parker 1983), the field strengths in the Hyades coronae must be one to two orders of magnitude greater than that in the solar corona. Our results suggest that the difference in the field strength may be the only significant difference between the Sun's corona and those of the Hyades.

The other parameter that the observations can place tight constraints on is the loop expansion factor Γ. This quantity is directly related to the form of the observed spectrum. It is well known that in hydrostatic loop models, the plasma temperature changes slowly along the loop, except for a thin transition region required at the loop base. The width of this transition region is typically very small compared to the loop length; thus to a good approximation the loop cross-sectional area throughout the transition region is equal to that at the base. This implies that the emitting area at the base of the corona (i.e., the top of the transition region) with a temperature of $\sim 10^6$ K is smaller by a factor Γ than that at T_{max}, $\sim 10^7$ K in our case. Hence the parameter Γ determines the relative amounts of material at high and low temperatures once T_{max} is specified, and consequently the form of the spectrum.

All the model fits indicate a small value for Γ, <3–4. This is a key result. This constrains the emitting loop to be relatively low-lying. Since a coronal loop is actually a magnetic flux tube, the loop expansion factor Γ is also equal to the ratio of the magnetic field strength at the loop base to that at the apex. A small value for Γ implies that the field decreases very little from base to apex. We expect this to hold only for loops with heights small compared to the size of their active region. The coronal magnetic field is generally believed to be due primarily to subphotospheric currents (Sheeley *et al.* 1975; Poletto *et al.* 1975; Levine 1976; Sheeley 1981): hence, the height scale over which the coronal field is expected to decrease is given by the horizontal extent of the field at the photosphere, or equivalently, by the size of the active region. In particular, since the size of the active region is clearly limited by the stellar radius, we conclude that the loop heights should be well below a stellar radius for loops of small Γ. This conclusion is consistent with the direct limits on L given in Table 6.

The final two parameters to be determined are the loop length L and the area filling factor f. Clearly, f has no effect on the form of the observed spectrum, but only on the absolute intensity. Unfortunately, to a large extent this is also true for L. In the loop models, once T_{max} and Γ are specified, the form of the differential emission measure is also completely specified in most cases. Only for loops with heights large compared to the gravitational scale height does the loop length begin to affect the emission measure distribution (e.g., Vesecky, Antiochos, and Underwood 1979; Serio *et al.* 1981). For the large values of T_{max} in our case, the scale height is large, ~ 5–8×10^{10} cm, which is of order the stellar radius; but we have already constrained the loop to be small compared to this scale, since unphysical values of f will result otherwise. Since L is constrained to a range of values such that it has a very minor effect on the form of the observed spectrum, it also affects only the absolute intensity. This explains the findings in the previous section that L and f cannot be independently constrained. A similar conclusion was also reached by Schmitt *et al.* (1985) for the case of Procyon.

We may, however, place better limits on L and f for stars that have been observed by *IUE* at the C IV transition region line formed at $T \approx 10^5$ K. Recall that in § I we noted that much of the UV line emission at $T \approx 10^5$ K or lower may be coming from cooler, non–X-ray emitting loops. However, the stellar surface flux in C IV coming from the bases of X-ray emitting loops must not be greater than the total C IV surface flux observed for the star. Thus the surface coverage factors derived from our loop models and UV and X-ray observations must satisfy the relation $f(\text{X-ray}) < f(\text{C IV}) < 1$.

Zolcinski *et al.* (1982) observed the two Hyades dwarf stars BD $+15°640$ and BD $+14°693$ with *IUE*. Bearing in mind that the C IV observations were not obtained simultaneously with the IPC observations, and hence we should allow for a factor of 2 or so uncertainty, we may use our loop model results in conjunction with the Zolcinski *et al.* (1982) surface fluxes and the line emissivity calculations of Raymond and Doyle (1981) to derive the fractional surface coverage required for the X-ray emitting loops to produce the observed C IV emission. By comparing these with the surface coverages predicted by the X-ray data alone, we can further constrain the range of allowable loop model parameters. This is shown for BD $+14°693$ and BD $+15°640$ in Figure 9, where we have f(X-ray) and f(C IV) for each star. The only region of parameter space that produces good model fits for the X-ray data as well as satisfying the constraints on surface coverage parameters lies in the lower left-hand portion of the plots for both stars. For BD $+14°693$, $L \lesssim 2 \times 10^{10}$ cm, and $1 \lesssim \Gamma \lesssim 2$, and $P \gtrsim 200$ dynes cm^{-2} constitutes the acceptable region, and for BD $+15°640$, roughly the same region is allowable, although loop models of constant cross section ($\Gamma \approx 1$) are acceptable for the latter star.

The ranges of loop parameters we give for BD $+15°640$ and

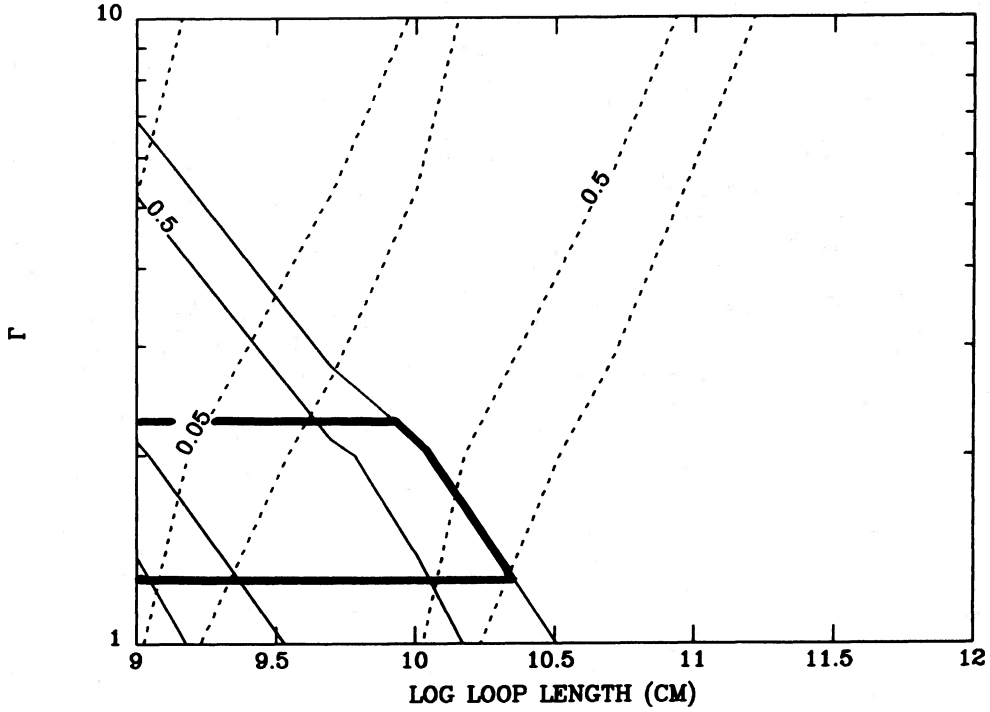

FIG. 9*a*

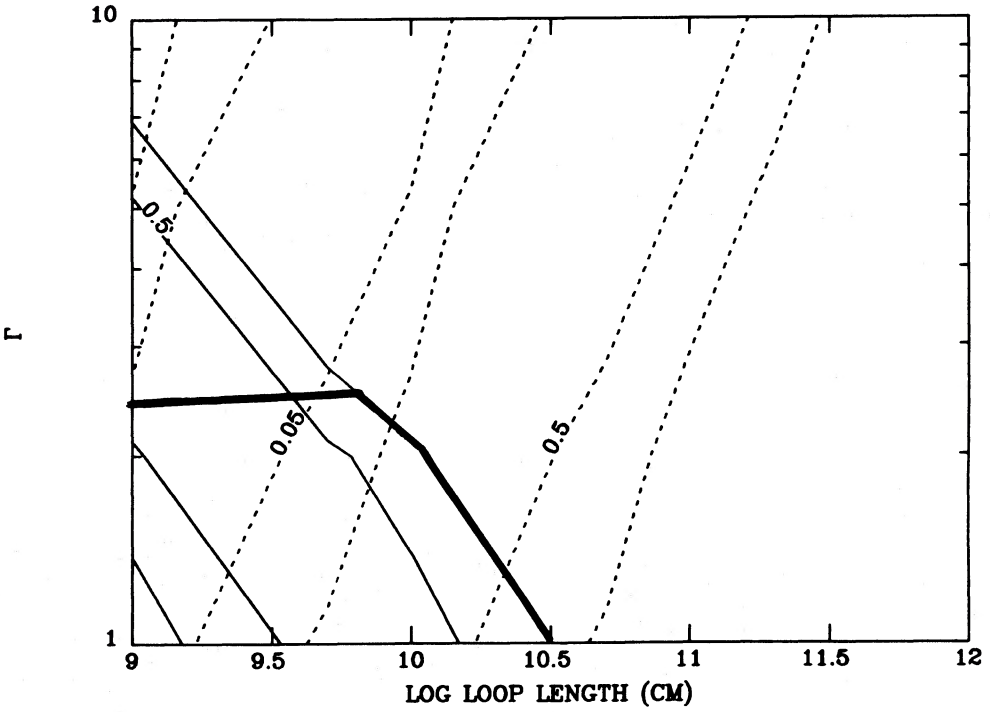

FIG. 9*b*

FIG. 9.—Contours of constant f(X-ray loops) (*dashed lines*) compared to f(C IV) (*thin solid lines*) for (*a*) BD +14°693 and (*b*) BD +15°640. The region where f(X-ray) < f(C IV) < 1 is shown by the thick solid line for each plot. In each case, 90% confidence upper limits for Γ have been used.

BD +14°693 are not particularly consistent with those derived by Zolcinski *et al.* (1982) and Landini *et al.* (1985) for the same stars. For example, the derived coronal (maximum) temperature for BD +15°640 ranges from 10^6 (Zolcinski *et al.*) to 5–7 × 10^6 (Landini *et al.*) to 15 × 10^6 K in our case. This is not too surprising, as the reprocessed IPC pulse height data were previously unavailable, and the above analyses required X-ray and UV line fluxes to arise from the same loops in order to estimate T_{max}. In our analysis T_{max} is determined from the X-ray spectra alone.

In summary, models with an X-ray loop surface coverage of $\lesssim 1$, and for two of the stars a C IV coverage below 1, require the maximum loop lengths and minimum base pressures given in Table 6. However, in light of our other results we believe that this is a very unlikely model for the Hyades coronae. The small value for Γ, and to some extent the large value for T_{max} coupled with expected limits on the sizes of stellar active regions discussed above, make it much more likely that both L and f are significantly smaller than the values in Table 6 and the base pressures commensurately larger. That is, our models are consistent with the picture of small ($<10^{10}$ cm), high-pressure coronal ($\gtrsim 400$ dynes cm^{-2}) loops covering a relatively small ($\lesssim 10\%$–20%) fraction of the stellar surface.

This picture is in accord with models of solar coronal heating in which the magnitude of the heating depends on the strength of the magnetic field: in this case, the X-ray emission from an ensemble of variously sized magnetic loops will be dominated by the emission from the smallest loops, where most of the coronal heating is occurring. In the case of the Sun, it is well known observationally that the smallest coronal loops are indeed those with the highest temperatures and pressures: the larger loops are generally associated with quiet Sun, not active regions or flares (Levine and Pye 1980; Pallavicini *et al.* 1981). Because the required X-ray surface flux is an order of magnitude or more than that seen on the Sun, the additional heat input drives up the coronal pressure to pressures comparable to solar flares, even in the largest loops. Thus, a reasonable scenario is that the X-ray emission from such active stars is primarily the result of high-pressure, "superactive" regions on the stellar disk.

The picture of a few strongly emitting loops dominating the disk integrated X-ray flux from stellar coronae, if it is correct, gives us some hope that the future of stellar X-ray observations may not be as bleak as one might suspect, given the lack of spatial resolution inherent in stellar observations. The flarelike pressures of such small hot loops should be verifiable by high-resolution X-ray spectroscopy of density-sensitive triplets from He-like ions formed at flarelike temperatures such as those observed with the X-ray polychromator on *SMM*: e.g., Ne IX, Mg XI, Si XIII, S XV (Wolfson *et al.* 1983; but see McKenzie 1985 for Ne IX blends). These ions all emit X-rays in the ~5–13 Å range, and their use as temperature and density diagnostics covers the T range ~4–15 × 10^6 K and $N_e \approx 10^{11}$–10^{14} cm^{-3}. An alternative would be to use similar density sensitive lines in the EUV or XUV, such as those of Fe IX–XV for $N_e \approx 10^9$–10^{11} cm^{-3} and Ca XV–XVI for $N_e \approx 10^{11}$ cm^{-3} and higher: such lines are in the 170–300 Å wavelength range and are formed at $T \approx 10^6$–10^7 K (Dere *et al.* 1979). In either case, high spectral resolution will be needed to resolve blends.

VII. CONCLUSIONS

We have successfully modeled the IPC pulse height spectra of active Hyades stars with single maximum temperature loop models. Although the spectra can also be formally modeled with a two-temperature (two isothermal components) model, the use of internally consistent hydrostatic loop models of a single maximum temperature offers advantages in the physical interpretation of the model results. We find in general that the X-ray pulse height spectra require a maximum temperature similar to that seen in solar flares. The constraint on loop area with height derived from the X-ray spectra suggests that active stellar loops are likely to be small ($L < 10^{10}$ cm), high-pressure ($\gtrsim 400$ dynes cm^{-2} base pressure), and covering only a small fraction ($<10\%$–20%) of the stellar surface, although their distribution over the stellar disk may be quite uniform. Future tests of such a scenario will involve the use of X-ray density diagnostics from He-like ions, or possible from density-sensitive EUV line ratios formed at $T > 10^6$ K.

We wish to thank Drs. J. H. M. M. Schmitt and S. Serio for their critical comments on the manuscript. The work of R. A. S. was supported by the *HEAO 2* Guest Investigator Program under contract NAS8-35873 and the Lockheed Independent Research Program. S. K. A. was supported by NASA grant NGR 05-020-668 at Stanford and by NASA contract DPR W-15367 at NRL. F. R. H. was supported by NASA contract NAS8-30751.

REFERENCES

Antiochos, S. K., and Noci, G. 1986, *Ap. J.*, **301**, 440.
Antiochos, S. K., and Sturrock, P. A. 1978, *Solar Phys.*, **49**, 359.
Athay, R. G. 1984, *Ap. J.*, **287**, 412.
Baliunas, S. L., *et al.* 1985, *Ap. J.*, **294**, 310.
Branch, D., Lambert, D. L., and Tomkin, J. 1980, *Ap. J. (Letters)*, **241**, L83.
Cash, W. 1976, *Astr. Ap.*, **52**, 307.
Catura, R. C., Acton, L. W., and Johnson, H. M. 1975, *Ap. J. (Letters)*, **196**, L47.
Dere, K. P., Mason, H. E., Widing, K. G., and Bhatia, A. K. 1979, *Ap. J. Suppl.*, **40**, 341.
Feldman, U. 1983, *Ap. J.*, **275**, 367.
Giacconi, R., *et al.* 1979, *Ap. J.*, **230**, 540.
Giampapa, M. S., Golub, L., Peres, G., Serio, S., and Vaiana, G. S. 1985, *Ap. J.*, **289**, 203.
Golub, L., Maxson, C., Rosner, R., Serio, S., and Vaiana, G. S. 1980, *Ap. J.*, **238**, 343.
Gorenstein, P., Harnden, F. R., Jr., and Fabricant, D. G. 1981, *IEEE Trans.*, **NS-28**, 869.
Harnden, F. R., Jr., Fabricant, D. G., Harris, D. E., and Schwarz, J. 1984, *Smithsonian Ap. Obs. Spec. Rept.*, No. 393.
Lampton, M., Margon, B., and Bowyer, S. 1976, *Ap. J.*, **208**, 177.
Landini, M., and Monsignori Fossi, B. C. 1975, *Astr. Ap.*, **42**, 213.
Landini, M., Monsignori Fossi, B. C., and Pallavicini, R. 1985, *Space Sci. Rev.*, **40**, 43.
Landini, M., Monsignori Fossi, B. C., Paresce, F., and Stern, R. A. 1985, *Ap. J.*, **289**, 709.
Levine, R. H. 1976, *Solar Phys.*, **46**, 159.
Levine, R. H., and Pye, J. P. 1980, *Solar Phys.*, **66**, 39.
Majer, P., Schmidt, J. H. M. M., Golub, L., Harnden, F. R., Jr., and Rosner, R. 1986, *Ap. J.*, **300**, 360.
Mewe, R., *et al.* 1982, *Ap. J.*, **260**, 233.
McKenzie, R. L. 1985, *Ap. J.*, **296**, 294.
Orral, F. Q., ed. 1981, *Solar Active Regions* (Boulder: Colorado Associated University Press).
Pallavicini, R., Peres, G., Serio, S., Vaiana, G., Golub, L., and Rosner, R. 1981, *Ap. J.*, **247**, 692.
Parker, E. N. 1983, *Ap. J.*, **264**, 642.
Peterson, D. M., Barm, R. L., Dunham, E., and Mink, D. 1981, *A.J.*, **86**, 1090.
Poletto, G., Vaiana, G. S., Zombeck, M. V., Krieger, A. S., and Timothy, A. F. 1975, *Solar Phys.*, **44**, 83.
Rabin, D., and Moore, R. 1984, *Ap. J.*, **285**, 359.
Raymond, J. C. 1979, unpublished.

Raymond, J. C., and Doyle, J. G. 1981, *Ap. J.*, **245**, 1141.
Raymond, J. C., and Smith, B. W. 1977, *Ap. J. Suppl.*, **35**, 419.
Rosner, R., Golub, L., Coppi, B., and Vaiana, G. S. 1978, *Ap. J.*, **222**, 317.
Rosner, R., Golub, L., and Vaiana, G. 1985, *Ann. Rev. Astr. Ap.*, **23**, 413.
Rosner, R., Tucker, W. H., and Vaiana, G. S. 1978, *Ap. J.*, **220**, 643.
Schmidt, J. H. H. M., Harnden, F. R., Jr., Peres, A., Rosner, R., and Serio, S. 1985, *Ap. J.*, **288**, 751.
Serio, S., Peres, G., Vaiana, G. S., Golub, L., and Rosner, R. 1981, *Ap. J.*, **243**, 288.
Sheeley, N. R. 1981, in *Solar Active Regions*, ed. F. Q. Orrall (Boulder: Colorado Associated Universities Press), p. 17.
Sheeley, N. R., Bohlin, J. D., Brueckner, G. E., Purcell, J. D., Scherrer, V., and Tousey, R. 1975, *Solar Phys.*, **40**, 103.
Stern, R. A. 1983, *Adv. Space Res.*, **2**, 39.
———. 1984, in *Proc. 3d Cambridge Workshop on Cool Stars, Stellar Systems, and the Sun*, ed. S. Baliunas and L. Hartmann (Springer: *Lecture Notes in Physics*, Vol. **193**), p. 150.
Stern, R. A., and Skumanich, A. 1983, *Ap. J.*, **267**, 232.
Stern, R. A., Underwood, J. H., and Antiochos, S. K. 1983, *Ap. J. (Letters)*, **264**, L55.
Stern, R. A., and Zolcinski, M. C. 1983, in *Activity in Red Dwarf Stars*, ed. P. B. Byrne and M. Rodono (Dordrecht: Reidel), p. 131.
Stern, R. A., Zolcinski, M. C., Antiochos, S. K., and Underwood, J. H. 1981, *Ap. J.*, **249**, 647.
Sturrock, P. A., and Uchida, Y. 1981, *Ap. J.*, **246**, 331.
Swank, J. H., White, N. E., Holt, S. S., and Becker, R. H. 1981, *Ap. J.*, **246**, 208.
Tucker, W. H. 1973, *Ap. J.*, **186**, 285.
Vaiana, G. S. 1983, in *IAU Symposium 102, Solar and Stellar Magnetic Fields: Origins and Coronal Effects*, ed. J. O. Stenflo (Dordrecht: Reidel), p. 165.
Vaiana, G. S., and Rosner, R., 1978, Ann. Rev. Astron. Astrophys., **16**, 393.
van Bueren, H. O. 1952, *Bull. Astr. Inst. Netherlands*, **11**, 385.
Vesecky, J. F., Antiochos, S. K., and Underwood, J. H. 1979, *Ap. J.*, **233**, 987.
Walter, F. M., Gibson, D. M., and Basri, G. 1983, *Ap. J.*, **267**, 665.
Wolfson, C. J., Doyle, J. G., Leibacher, J. W., and Phillips, K. J. H. 1983, *Ap. J.*, **269**, 319.
Zolcinski, M. C., Antiochos, S. K., Walker, A. B. C., and Stern, R. A. 1982, *Ap. J.*, **258**, 177.
Zolcinski, M. C., and Stern, R. A. 1985, paper presented at ESA Workshop on X-ray Spectroscopy in Space.

S. K. ANTIOCHOS: Code 4170, Naval Research Laboratory, Washington, DC 20375

F. R. HARNDEN, JR.: Harvard-Smithsonian Center for Astrophysics, 60 Garden St., Cambridge, MA 02138

R. A. STERN: Department 91-20, Building 255, Lockheed Palo Alto Research Laboratory, 3251 Hanover St., Palo Alto, CA 94304